انقذ الاطفال

A 700 GeV Higgs Resonance: Motivations, Experiment, and Unitarity

(cf. arXiv:2308.01429 [hep-ph])

George Rupp*

CeFEMA/IST Lisbon

- Introduction: non-perturbative approach to Φ^4 theory
- Indications from lattice simulations
- Experimental signals in ATLAS and CMS data
- Unitary coupled-channel formalism for $h(125)+H(700)$
- Summary and Conclusions

*With thanks to **M. Consoli**, L. Cosmai, and F. Fabbri

I. Introduction: non-perturbative approach to ϕ^4 theory

- In the usual perturbative $\lambda\phi^4$ theory, λ and so also the effective potential $\mathbf{V_{eff}(\phi)}$, normalised to vanish at $\phi = \mathbf{v} = \mathbf{246\,GeV}$, become negative again at $\sim \mathbf{10^{10}\,GeV}$);
  (cf. E. Gabrielli *et al.*, PRD **89** (2014) 053012).
- Thereabove, $\mathbf{V_{eff}(\phi)}$ has a new minimum at $\sim \mathbf{10^{31}\,GeV}$, well beyond the Planck scale and much deeper than the EW vacuum;
  (cf. V. Branchina, E. Messina *PRL* **111** *(2013) 241801*).
- It is unclear whether gravitational effects can become strong enough to stabilise the potential, so most authors accept metastability as a possible scenario in a cosmological perspective, with a tunnelling time much longer than the estimated lifetime of the universe.
- Explaining why the theory remains trapped in our EW vacuum would require to control the properties of matter in the extreme conditions of the early universe.

- Alternatively, we can consider a non-perturbative approach to $\lambda\phi^4$ theory, inspired by the seminal article *"Radiative Corrections as the Origin of Spontaneous Symmetry Breaking"*, S Coleman, E. Weinberg, PRD **7** (1973) 1888. In this paper, it is shown that spontaneous symmetry breaking (SSB) can originate in the zero-point energy (ZPE) (see Figure 1) of field fluctuations in the classically scale-invariant limit $\mathbf{V''_{eff}(\phi = 0) \rightarrow 0^+}$.
- Note that in the perturbative CW approach, a first-order SSB scenario could only work in the presence of gauge bosons, in order to compensate for the large ZPE due to the ϕ field, provided that $\boldsymbol{\lambda \sim \mathcal{O}\, g^4_{gauge}}$.
- However, contrary to the Coleman-Weinberg (CW) mechanism of perturbatively improving the simple one-loop potential for a massless theory, our approach is based on non-perturbative approximations to the effective potential that are all consistent with triviality.

- These approximations, in the framework of especially the one-loop and Gaussian effective potentials, resum to all orders different classes of diagrams yet being physically equivalent. This means that they result in the same structure of the effective potential, up to terms that vanish in the continuum limit.
- In such a non-perturbative picture, the ϕ^4 interaction is not always repulsive. Besides the $+\lambda\delta^{(3)}(\vec{\mathbf{r}})$ tree-level repulsion in the symmetric phase, there is also a $-\lambda^2\,\mathbf{exp}(-2\mathbf{m}_\phi\mathbf{r})/\mathbf{r}^3$ attraction from the ultraviolet-finite part of the one-loop diagrams, with increasing range in the $\mathbf{m}_\phi \to \mathbf{0}$ limit;
  (cf. M. Consoli, P. M. Stevenson, IJMPA **15** (2000) 133).
- To consistently include higher-order effects of opposite sign, one should rearrange the perturbative expansion by symmetrically renormalising both the contact repulsion and the long-range attraction. Thus, for a small enough $\mathbf{m_\Phi} > \mathbf{0}$, the attractive tail dominates and the lowest-energy state is not the trivial, empty vacuum with $\phi = \mathbf{0}$, but a state with $\phi \neq \mathbf{0}$ and a Bose condensate of symmetric-phase quanta in the $\vec{\mathbf{k}} = \vec{\mathbf{0}}$ mode;
  (cf. P. M. Stevenson, MPLA **24** (2009) 261).

Concretely, with $\mathbf{M(\phi)^2 \equiv \lambda\phi^2/2}$ standing for the ZPE of free-field fluctuations, the one-loop effective potential reads

$$\mathbf{V_{1\text{-}loop}(\phi) = \frac{\lambda\phi^4}{4!} - \frac{M^4(\phi)}{64\pi^2} \ln \frac{\Lambda^2\sqrt{e}}{M^2(\phi)}} \ , \tag{1}$$

with $\mathbf{\Lambda}$ the ultraviolet cutoff. The Gaussian effective potential, which resums all one-loop bubbles, preserves the same structure, up to terms that vanish for $\mathbf{\Lambda \to \infty}$. Denoting by $\mathbf{\phi_v}$ the minimum of $\mathbf{V_{1\text{-}loop}(\phi)}$ and $\mathbf{M_H \equiv M(\phi_v)}$, we get

$$\mathbf{V_{eff}(\phi_v) = V_{1\text{-}loop}(\phi_v) = -\frac{M_H^4}{128\pi^2}} \ , \quad \mathbf{M_H^2 \sim \lambda\phi_v^2 \sim \Lambda^2 e^{-1/\lambda}}. \tag{2}$$

Important: the vacuum energy is invariant under the renormalisation group, so $\mathbf{M_H}$ does not depend on the cutoff $\mathbf{\Lambda}$. Thus, $\mathbf{\lambda \sim L^{-1}}$, with $\mathbf{L \equiv \ln(\Lambda/M_H)}$, vanishes in the continuum limit ('triviality').

This results in a very interesting pattern of scales:

$$\lambda \sim L^{-1} \ , \quad m_h^2 = V''_{eff}(\phi_v) \sim v^2 L^{-1} \ , \quad M_H^2 \sim L\, m_h^2 = K^2 v^2 \ , \tag{3}$$

where K is a cutoff-independent constant and

$$\phi_v^2 \ \equiv \ Z_\phi v^2 \ , \quad \text{with} \quad Z_\phi \ = \ (M_H/m_h)^2 \sim L \ . \tag{4}$$

A possible first indication of the actual mass of such a heavy Higgs boson may come from lattice calculations referred in

C. B. Lang, NATO Sci. Ser. C **449** (1994) 133 [hep-lat/9312004].

Found upper bound on the Higgs mass: $M_H^{max} = 670\,(80)$ **GeV**.

Recommended further reading on non-perturbative ϕ^4 theory:

M.C., L.Cosmai, Int. J. Mod. Phys. **A35** (2020) 2050103; hep-ph/2006.15378

M.C., L.Cosmai, Symmetry **12** (2020) 2037; doi:103390/sym12122037

M.C. , in Veltman Memorial Volume, Acta Phys. Pol. **B52** (2021) 763; hep-ph/2106.06543

M.C., L.Cosmai, Int. J. Mod. Phys. **A37** (2022) 2250091; arXiv:2111.08962v2 [hep-ph]

M.C., L.Cosmai, F. Fabbri, arXiv:2208.00920v2 [hep-ph], revised December 2022

M.C., L.Cosmai, F.Fabbri, Universe **9** (2023) 99; MDPI Special Issue: Higgs and BSM Physics

Figure 1

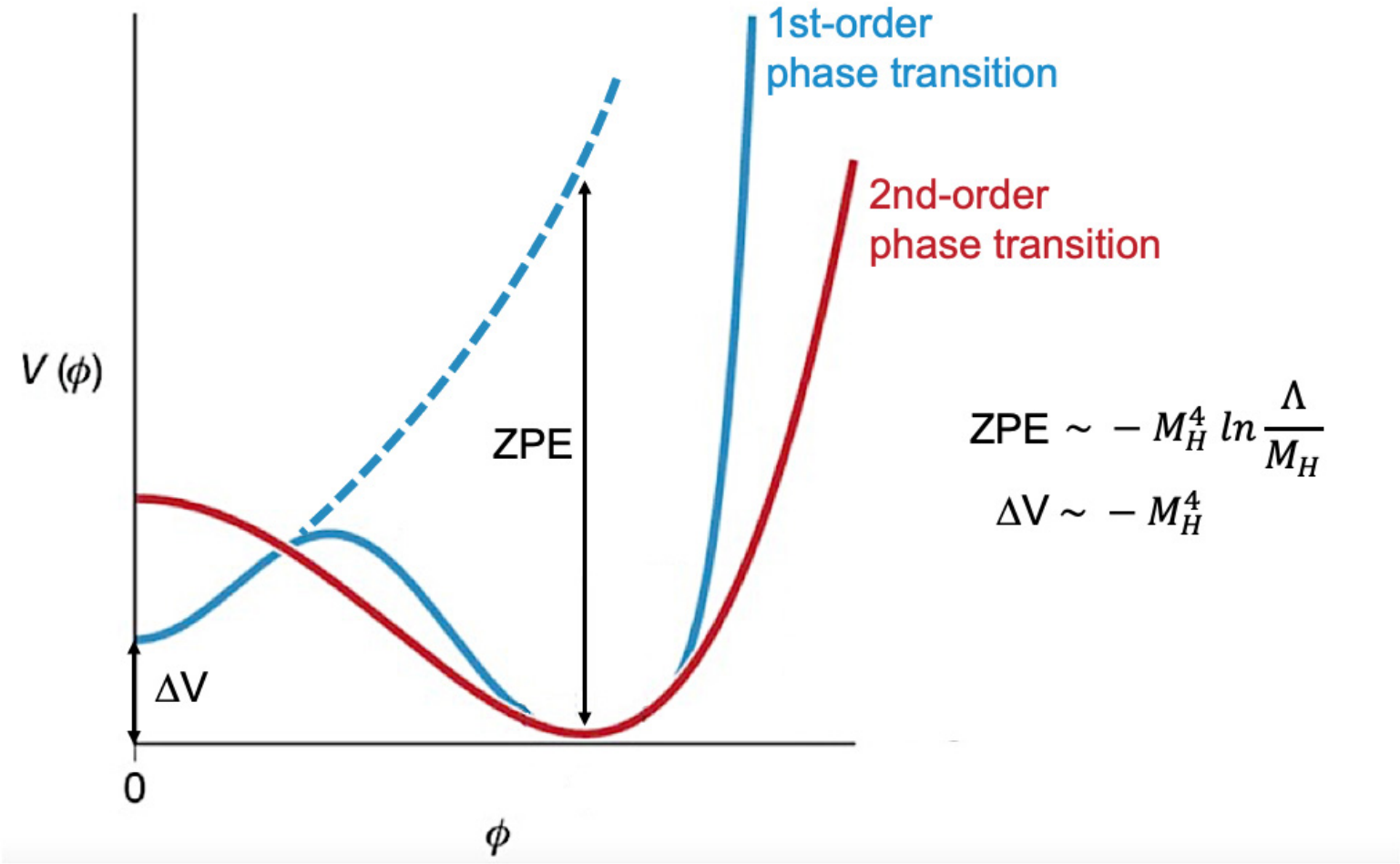

An intuitive picture that illustrates the crucial role of the zero-point energy in a first-order scenario of spontaneous symmetry breaking. Differently from the standard second-order picture, it has to compensate for a tree-level potential with no non-trivial minimum.

II. Indications from lattice simulations

- A first indication may come from lattice simulations of the four-dimensional ferromagnetic Ising model, showing a weak first-order phase transition for the internal energy and the magnetisation; see S. Akiyama *et al.*, Phys. Rev. D **100** (2019) 054510.
- Next we revisit detailed results of another lattice simulation, viz. in the symmetric and the broken phase of **4D Φ^4** theory, also in the Ising limit and very close to the critical coupling κ_c; see M. Consoli, L. Cosmai, IJMPA **35** (2020) 2050103 [2006.15378].
- Figure 2 shows data for the rescaled propagator $G(\hat{p})\,(\hat{p}^2 + m^2)$ as a function of the lattice momentum squared $\hat{p}^2$, for κ close to yet below κ_c. We see that the mass fitted from high momenta perfectly describes the data down to $\hat{p} = 0$.
- Figures 3 and 4 show similar data, but now for κ just slightly above κ_c. In Fig. 3 and the inset for low momenta, the data were rescaled with a lattice mass M_H obtained from a fit to all data with $\hat{p} > 0.1$. Figure 4 displays data for very low momenta and rescaled with the lattice mass m_h for $\hat{p} = 0$.

Figure 2

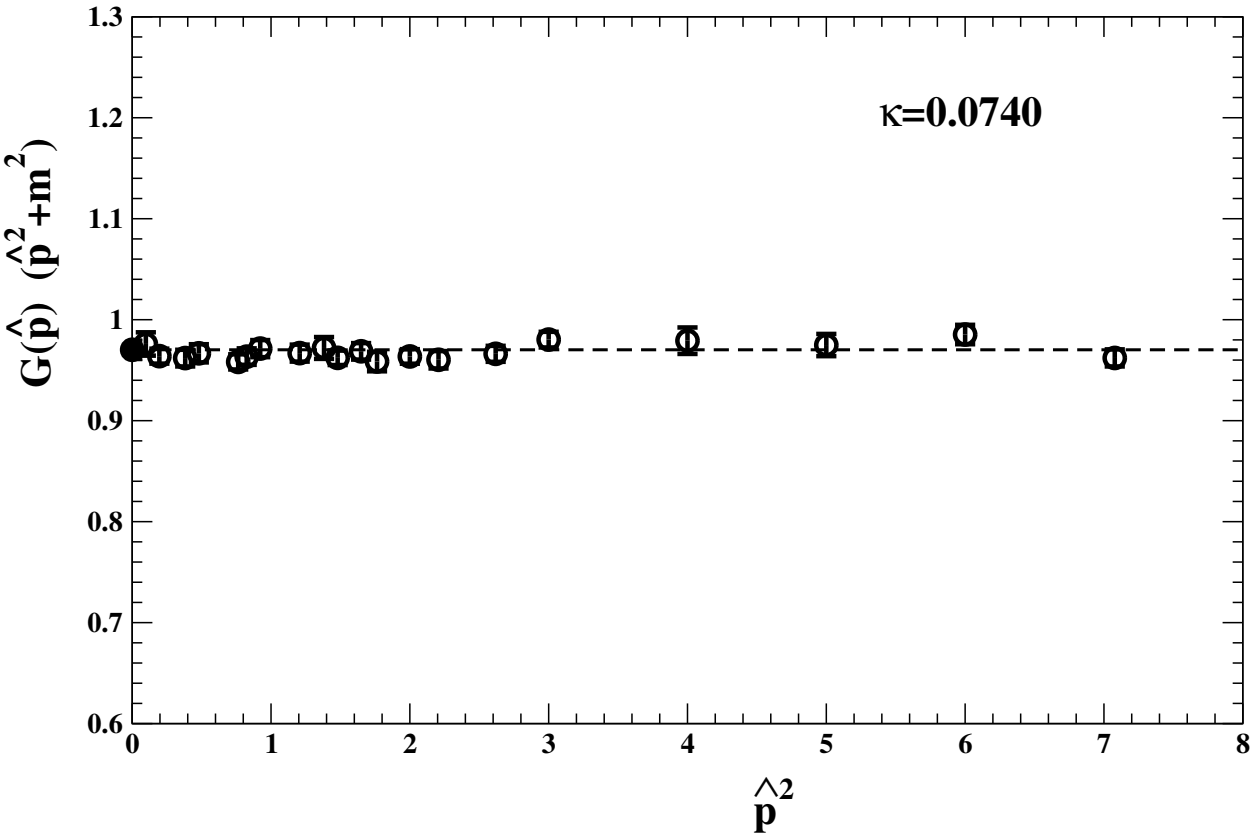

The lattice data from M. Consoli, L. Cosmai, Int. J. Mod. Phys. A **35** 2050103 (2020) [2006.15378] for the rescaled propagator in the symmetric phase at $\kappa = 0.074$, as a function of the lattice momentum squared $\hat{p}^2$. The fitted mass from high $\hat{p}^2$, viz. $m_{\rm latt} = 0.2141\,(28)$, describes the data well, down to $\hat{p} = 0$.

Figure 3

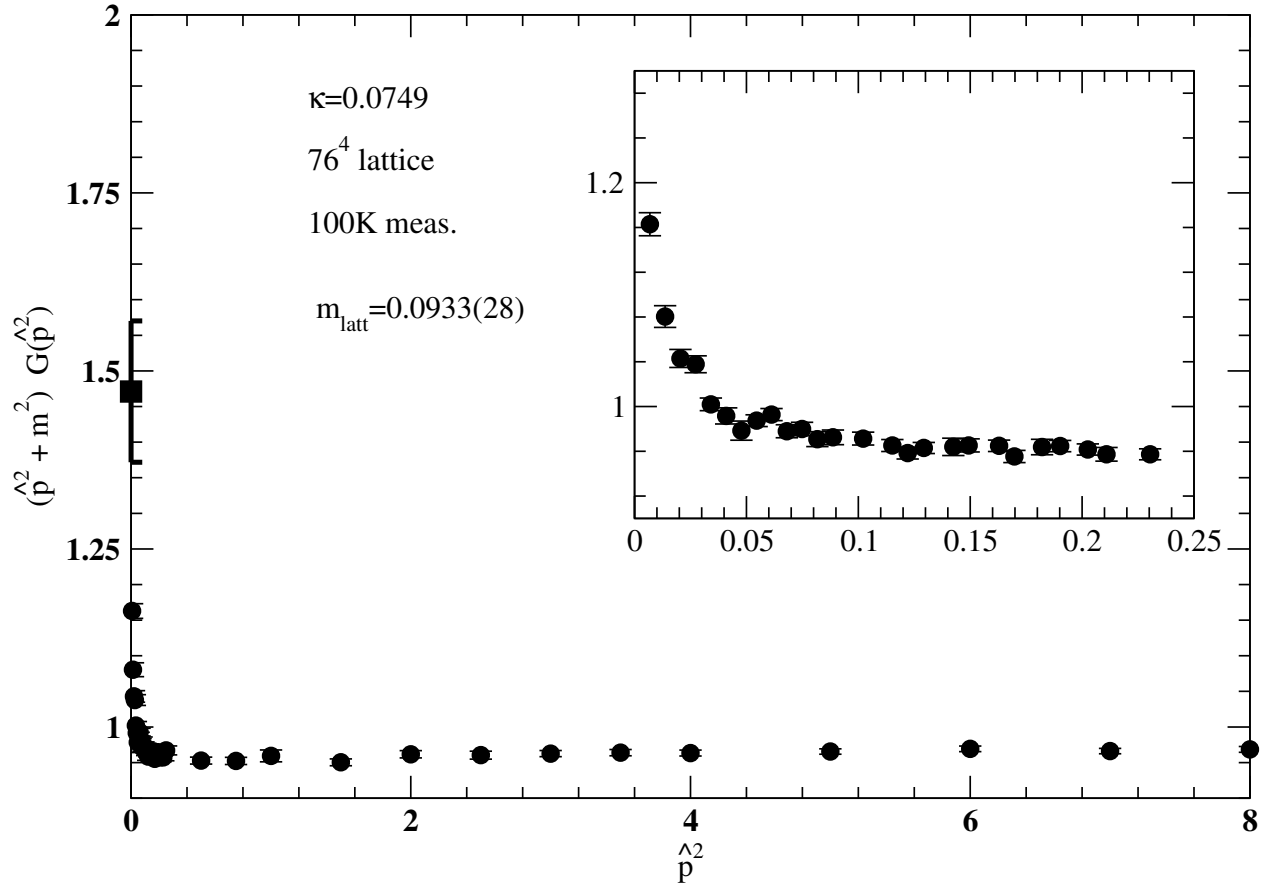

The propagator data from M. Consoli, L. Cosmai, Int. J. Mod. Phys. A **35** 2050103 (2020) [2006.15378], for $\kappa = 0.0749$, rescaled with the lattice mass $M_H \equiv m_{\rm latt} = 0.0933\,(28)$ obtained from the fit to all data with $\hat{p}^2 > 0.1$. The peak at $p = 0$ is $M_H^2/m_h^2 = 1.47\,(9)$, as computed from the fitted M_H and the zero-momentum mass $m_h = 0.0769\,(8)$.

Figure 4

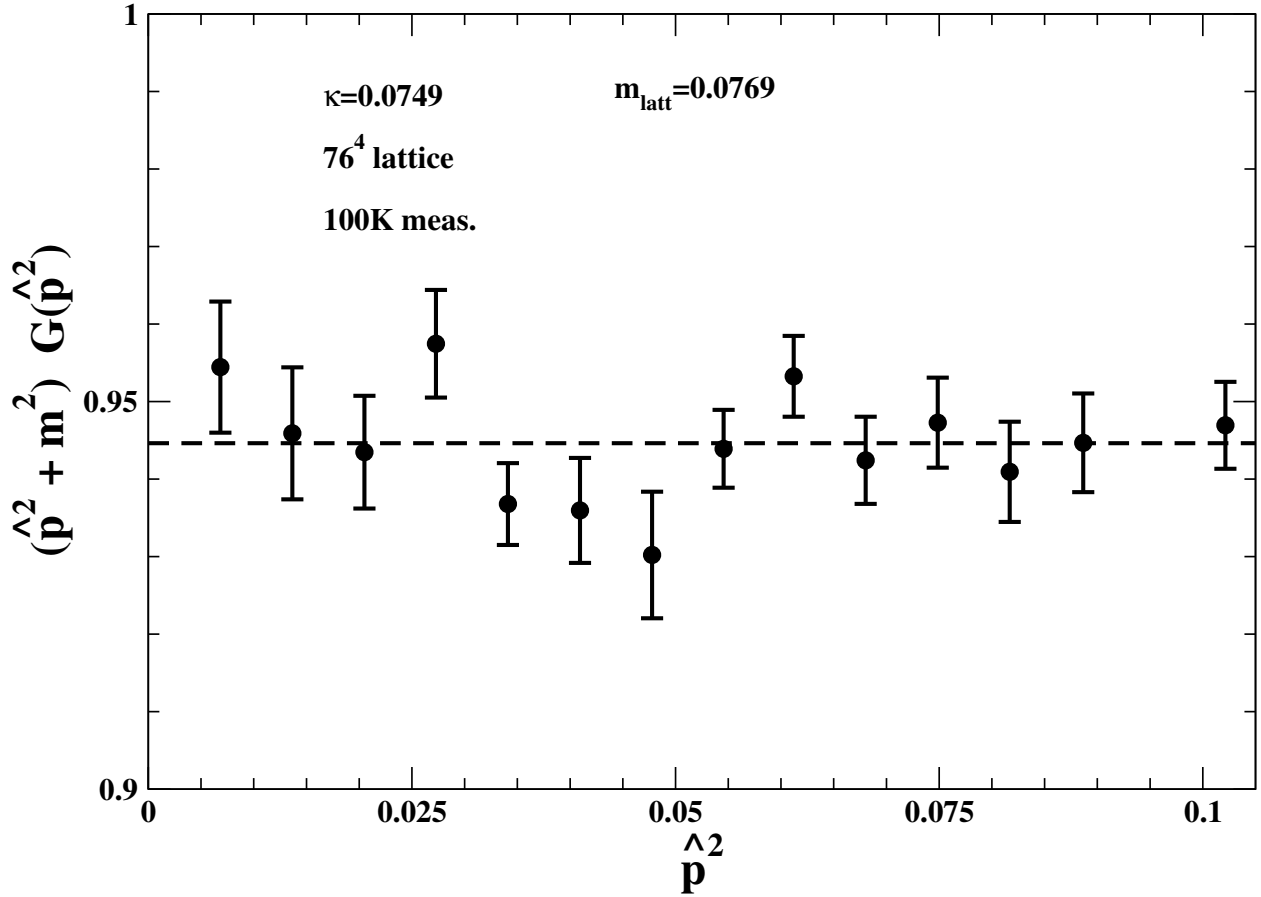

The propagator data from M. Consoli, L. Cosmai, Int. J. Mod. Phys. A **35** 2050103 (2020) [2006.15378], at $\kappa = 0.0749$ for $\hat{p}^2 < 0.1$. The lattice data were rescaled here with zero-momentum mass $m_h = 0.0769\,(8)$.

- Especially Fig. 3 suggests a weak first-order phase transition, like in Phys. Rev. D **100** (2019) 054510, besides a more complicated structure than just a single propagator pole for $\hat{\mathbf{p}} \to \mathbf{0}$.

- Thus, a two-mass propagator form was used to fit the data, i.e.,

$$\mathbf{G(p)} \;=\; \frac{\mathbf{1-I(p)}}{\mathbf{2}}\,\frac{\mathbf{Z_h}}{\mathbf{p^2+m_h^2}} \;+\; \frac{\mathbf{1+I(p)}}{\mathbf{2}}\,\frac{\mathbf{Z_H}}{\mathbf{p^2+M_H^2}}\;, \qquad (5)$$

  with $\mathbf{I(p)}$ an interpolating function depending on an intermediate momentum scale $\mathbf{p_0}$ and tending to $\mathbf{+1}$ for large $\mathbf{p^2 \gg p_0^2}$ and to $\mathbf{-1}$ when $\mathbf{p^2 \to 0}$; see
  M. Consoli, Acta Phys. Polon. B **52** (2021) 763.

- Fit to the quantities in Eqs. (3) and (4) (details in 0823.01429):

$$\mathbf{(M_H)^{Theor} \;=\; 690 \pm 10\,(stat) \pm 20\,(sys)\;GeV}\;. \qquad (6)$$

- Note that Eqs. (3) and (4) imply $\mathbf{m_h \ll M_H}$ for very large $\mathbf{\Lambda}$, with $\mathbf{M_H}$ independent of $\mathbf{\Lambda}$. So for decreasing $\mathbf{\Lambda}$, $\mathbf{(m_h)^{max} \to M_H}$, thus being compatible with the upper bound $\mathbf{M_H^{max} = 670\,(80)\;GeV}$ found for the single-Higgs lattice simulation in C. B. Lang, NATO Sci. Ser. C **449** (1994) 133.

III. Experimental signals in ATLAS and CMS data

- Before we look at the data, we should clarify what kind of signals we may expect for a heavy Higgs. Now, in the conventional perturbative approach one would expect a width of several to many hundreds of GeV for decays to e.g. $\mathbf{W^{\pm}W^{\mp}}$, $\mathbf{ZZ}$, and $\mathbf{hh}$, resulting from a tree-level coupling $\boldsymbol{\lambda_0 = 3M_H^2/v^2}$.
- However, since our $\mathbf{M_H}$ is derived from the non-perturbative $\mathbf{M_H}$ effective potential and not from the quadratic shape of the tree-level potential in the Lagrangian, the coupling is rescaled as

$$\lambda(\mathbf{v}) \;=\; \frac{\mathbf{3M_H^2}}{\phi_{\mathbf{v}}^2} \;=\; \frac{\mathbf{3m_h^2}}{\mathbf{v^2}} \;=\; \frac{\mathbf{m_h^2}}{\mathbf{M_H^2}}\,\lambda_0\,. \qquad (7)$$

  For further discussion, see
  0823.01429 and J. Bagger, C. Schmidt, PRD **41** (1990) 264.
- Therefore, we should expect partial decay widths of only a few GeV for $\mathbf{H \to W^{\pm}}$, $\mathbf{ZZ}$, $\mathbf{hh}$, in the case of a heavy Higgs with a mass of about **700 GeV**. Thus, the decay $\mathbf{H \to t\bar{t}}$ would be dominant, with a width of several tens of GeV.

- First we look at the ATLAS 4-lepton data in Fig. 5. Now, an accurate description of the ATLAS background can be obtained in terms of a power law $\mathbf{N_b(E) \sim A \times (710\ GeV/E)^{\nu}}$, with $\mathbf{A \sim 10.55}$ and $\boldsymbol{\nu \sim 4.72}$. Then, by simple redefinitions, the theoretical number of events can be expressed as

$$\mathbf{N_{TH}(E) \;=\; N_b(E) + \frac{P^2 + 2P\,x(E)\,\sqrt{N_b(E)}}{\gamma_H^2 + x^2(E)}}\ , \qquad (8)$$

where $\mathbf{x(E) = (M_H^2 - E^2)/M_H^2}$, $\mathbf{P \equiv \gamma_H \sqrt{N_R}}$, and $\mathbf{N_R = \sigma_R \times \mathcal{A} \times 139\ fb^{-1}}$ denotes the extra events at the resonance peak, for an acceptance $\boldsymbol{\mathcal{A}}$.

- In another ATLAS paper, the differential 4-lepton cross section $\mathbf{\langle d\sigma/dE \rangle}$, with $\mathbf{E = m(4l)}$, is reported in the same energy region, showing the same type of excess-defect sequence as in Table 2; see Fig. 6 and Table 4.

Figure 5

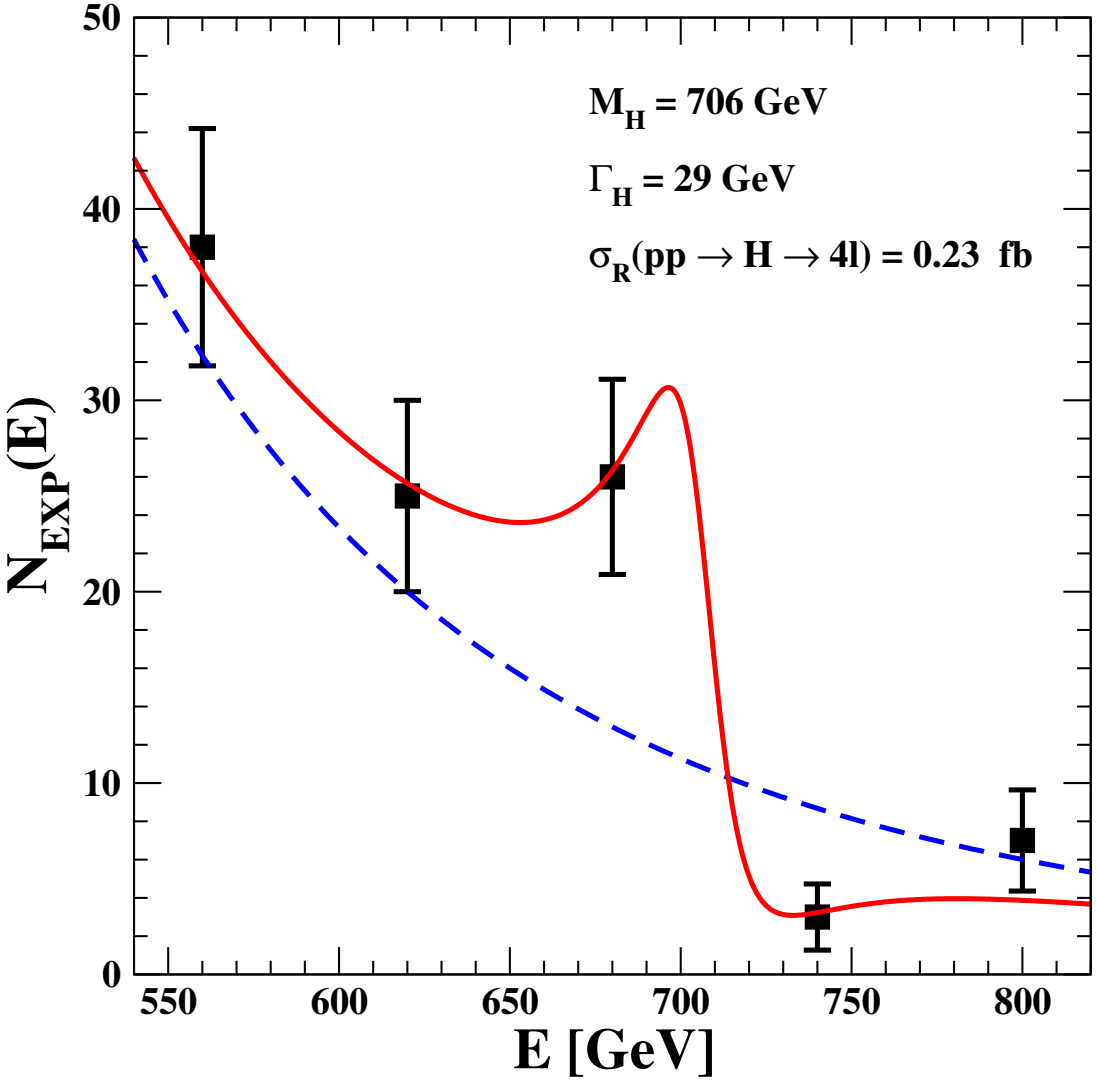

The values $\mathrm{N_{EXP}(E)}$ in Table 2 for ATLAS [1] data vs. the corresponding $\mathrm{N_{TH}(E)}$ in Eq. (8) (solid red curve). The resonance parameters are $M_H = 706$ GeV, $\gamma_H = 0.041$, $\sigma_R = 0.23$ fb and the ATLAS background (dashed blue curve) is approximated as $N_b(E) = A \times (710\ \mathrm{GeV}/E)^{\nu}$, with $A = 10.55$ and $\nu = 4.72$.

[1] Eur. Phys. J. C **81**, 332 (2021)

Table 2. For a luminosity of 139 fb^{-1}, we report the observed ATLAS [52] ggF-low events $N_{EXP}(E)$ and the corresponding estimated background $N_B(E)$ in the range of invariant mass $m4l = E = 530 \div 830$ GeV. In view of the considerable difference in the energy resolution of the various types of four-lepton events, to avoid spurious migrations between neighbouring bins, we have grouped the data into larger bins of 60 GeV, centred at 560, 620, 680, 740, and 800 GeV. These correspond to the 10 bins of 30 GeV, from 545 (15) GeV to 815 (15) GeV; see Ref. [52]. In this energy range, the uncertainties in the background are below 5% and have been neglected. The statistical errors of $N_{EXP}(E)$ are not reported by ATLAS and will be assumed to be given by $\sqrt{N_{EXP}}$, as for a Poisson distribution.

E [GeV]	$N_{EXP}(E)$	$N_B(E)$	$N_{EXP}(E) - N_B(E)$
560 (30)	38±6.16	32.0	6.00 ± 6.16
620 (30)	25±5.00	20.0	5.00 ± 5.00
680 (30)	26±5.10	13.04	12.96 ± 5.10
740 (30)	3±1.73	8.71	-5.71 ± 1.73
800 (30)	7±2.64	5.97	1.03 ± 2.64

Figure 6

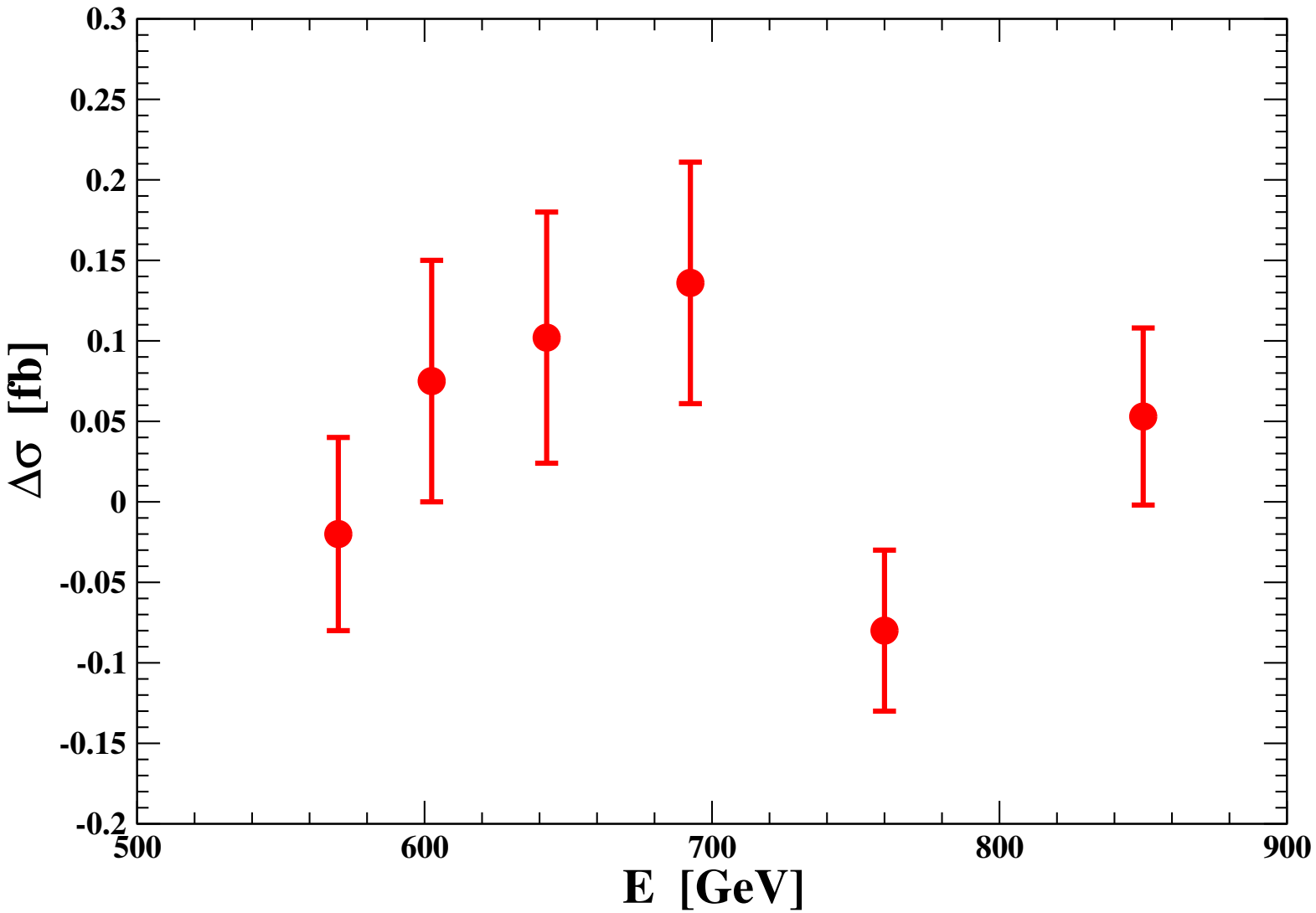

The quantity $\Delta\sigma = (\sigma_{\rm EXP} - \sigma_{\rm B})$ reported for each bin in the last column of Table 4, for the ATLAS data of JHEP **07**, 005 (2021).

Table 4. The observed ATLAS [53] cross section and the estimated background in the range of four-lepton invariant mass $m(4l) \equiv E$ from 555 to 900 GeV. These values have been obtained by multiplying the bin size with the average differential cross sections $\langle (d\sigma/dE) \rangle$, reported for each bin in the companion HEPData file. Besides the non-resonant $gg \to 4l$ process, the background cross section σ_B contains the dominating contributions from $q\bar{q} \to 4l$ events (as well as from other sources).

.

Bin [GeV]	$\sigma_{\rm EXP}$ [fb]	$\sigma_{\rm B}$ [fb]	$(\sigma_{\rm EXP} - \sigma_{\rm B})$ [fb]
555–585	0.252 ± 0.056	0.272 ± 0.023	-0.020 ± 0.060
585–620	0.344 ± 0.070	0.259 ± 0.021	$+0.085 \pm 0.075$
620–665	0.356 ± 0.075	0.254 ± 0.023	$+0.102 \pm 0.078$
665–720	0.350 ± 0.073	0.214 ± 0.019	$+0.136 \pm 0.075$
720–800	0.126 ± 0.047	0.206 ± 0.018	-0.080 ± 0.050
800–900	0.205 ± 0.052	0.152 ± 0.017	$+0.053 \pm 0.055$

- In Fig. 7 we now display 2-photon data, given in Table 5, for a similar energy region as in Fig. 6 and from the same ATLAS paper. The employed fit expression from the referred Eq. (44) in 0823.01429 is too complicated to be discussed here. For details, see the e-print.
- Figure 8 shows three different fits to the above ATLAS 2-photon data in Table 5, employing the same Eq. (44) from 0823.01429. The three cases correspond to a width of the proposed heavy Higgs of **15**, **25**, and **35 GeV**.
- Figure 9 shows CMS data of the cross section for the process

$$\sigma(\mathbf{full}) \;=\; \sigma(\mathbf{pp} \to \mathbf{X} \to \mathbf{hh} \to \mathbf{b\bar{b}} + \gamma\gamma) \;, \qquad (8)$$

in a search for new resonances decaying, through a pair of $\mathbf{h} = \mathbf{h(125)}$ scalars, into the particular final state made up of a $\mathbf{b\bar{b}}$ pair and a $\gamma\gamma$ pair. For a spin-zero resonance, the **95%** upper limit $\sigma(\mathbf{full}) < \mathbf{0.16}$ fb, for an invariant mass of **600 GeV**, was found to increase by about a factor of two, up to $\sigma(\mathbf{full}) < \mathbf{0.30\ fb}$, on a plateau of $\mathbf{650 \div 700\ GeV}$, and then to decrease for higher energies.

Figure 7

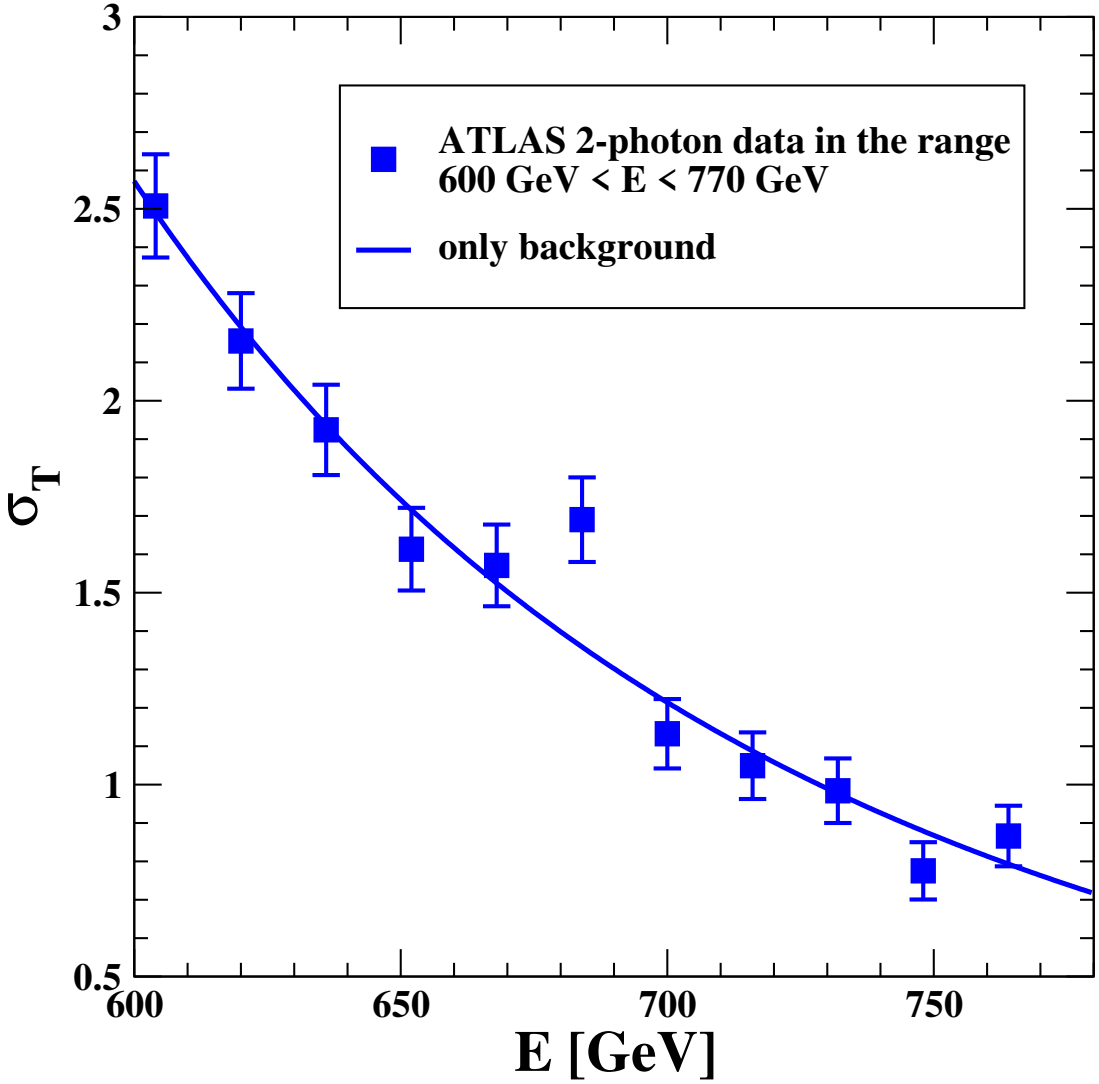

The fit with Eq. (44) and $\sigma_R = 0$ to the ATLAS [2] data in Table 5, converted to cross sections in fb. The chi-squared value is $\chi^2 = 14$, with the background parameters $A = 1.35$ *fb* and $\nu = 4.87$.

[2] JHEP **007**, 005 (2021)

Table 5. The ATLAS [53] experimental cross section $\hat{\sigma}_{\rm EXP}$ from Eq. (46) for each energy bin. The two cross sections $\sigma_{\rm EXP}$ and $\sigma_{\rm B}$ are given in Table 4. The other background cross section $\sigma_{\rm B}^{\rm gg}$ only takes into account the non-resonant $gg \to 4l$ process and was computed by multiplying the bin size with the average differential cross section ($d\sigma_{\rm B}^{\rm gg}/{\rm dE}$) in each bin. The central value of $\hat{\sigma}_{\rm EXP}$ in the second column of the 720–800 GeV bin is negative, because the expected background in Table 4, from $q\bar{q} \to 4l$ events (as well as from other sources), is larger than the experimental value itself.

Bin [GeV]	$\hat{\sigma}_{\rm EXP}$ [fb]	$\sigma_{\rm B}^{\rm gg}$ [fb]	$(\hat{\sigma}_{\rm EXP} - \sigma_{\rm B}^{\rm gg})$ [fb]
555–585	0.003 ± 0.060	0.023 ± 0.004	-0.020 ± 0.060
585–620	0.105 ± 0.073	0.020 ± 0.003	$+0.085 \pm 0.075$
620–665	0.121 ± 0.078	0.019 ± 0.003	$+0.102 \pm 0.078$
665–720	0.152 ± 0.075	0.016 ± 0.003	$+0.136 \pm 0.075$
720–800	-0.067 ± 0.050	0.013 ± 0.002	-0.080 ± 0.050
800–900	0.062 ± 0.055	0.009 ± 0.002	$+0.053 \pm 0.055$

Figure 8

Fit with interference of a background + resonance

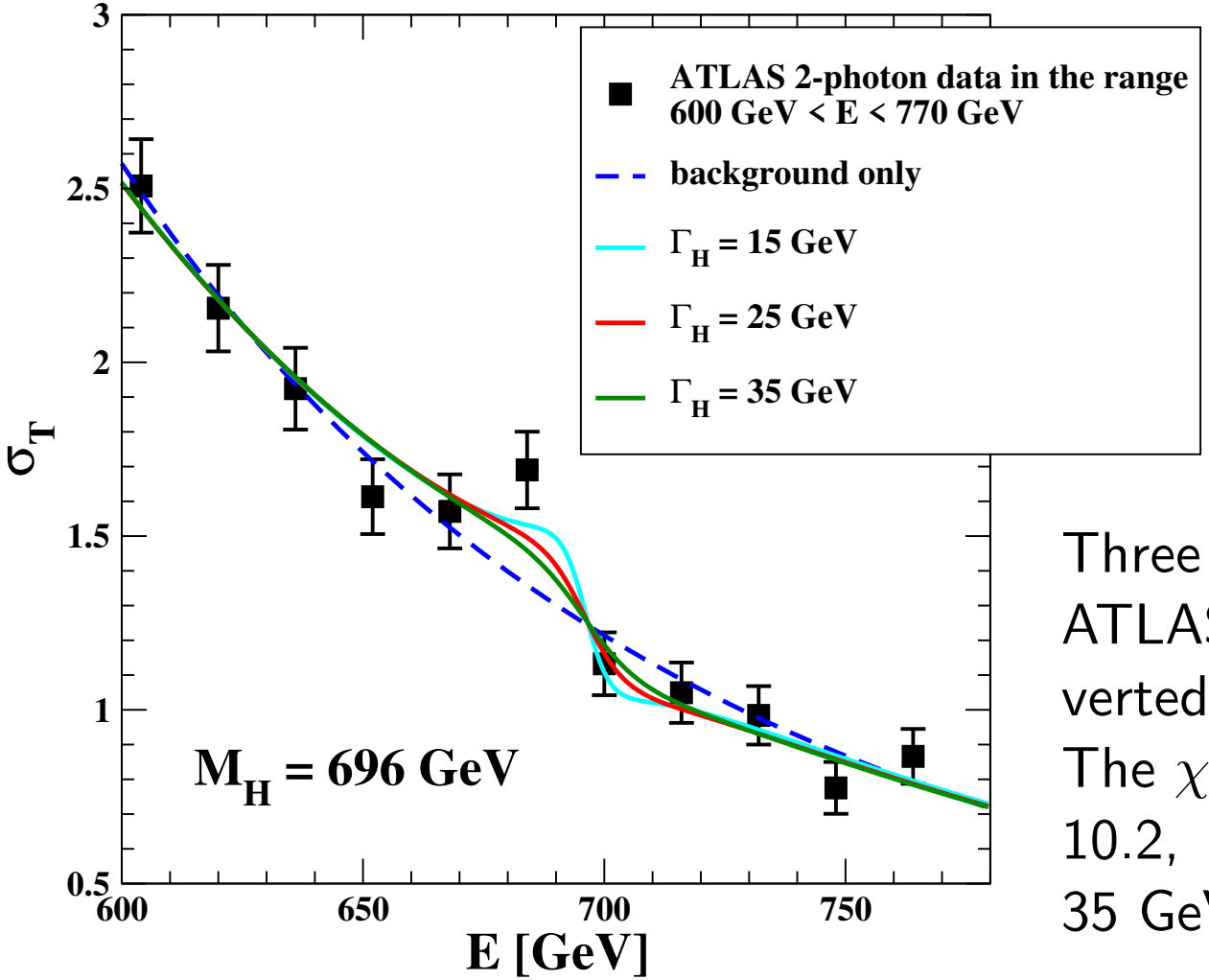

Three fits with Eq. (44) to the ATLAS [2] data in Table 5, converted to cross sections in fb. The χ^2 values are 7.5, 8.8, and 10.2, for $\Gamma_H = 15$, 25, and 35 GeV, respectively.

[2] JHEP **007**, 005 (2021)

Figure 9

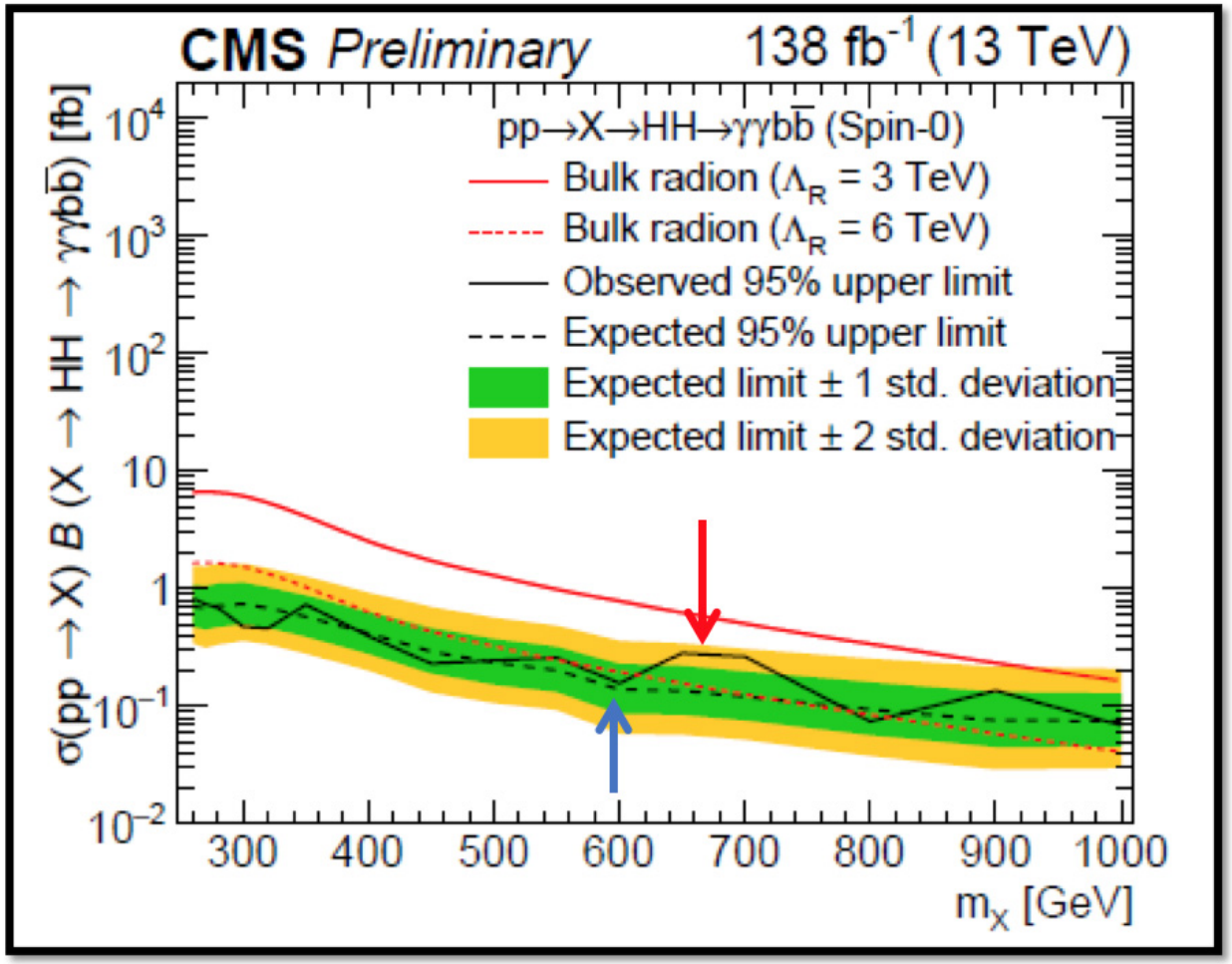

Expected and observed 95% upper limit for the cross section $\sigma(pp \to X \to h(125)h(125) \to b\bar{b} + \gamma\gamma)$ observed by the CMS Collaboration in CERN Report no. CMS-PAS-HIG-21-011.

- In Fig. 10 we show data analogous to those in Fig. 9, but now produced by ATLAS. Again, one finds a modest $\mathbf{1.2\sigma}$ excess at $\mathbf{650\,(25)\ GeV}$, followed immediately by a $\mathbf{1.4\sigma}$ defect, which might indicate a negative above-peak $\mathbf{(M_H^2 - s)}$ interference effect like that found in the ATLAS 4-lepton data. From the observed value $\boldsymbol{\sigma(pp \to H \to hh) < 150\ fb}$, this gives $\mathbf{B(H \to hh) < 0.15}$, so compatible with CMS. As the 3-body decays $\mathbf{H \to hhh}$, $\mathbf{H \to hW^+W^-}$, and $\mathbf{H \to hZZ}$ should only give a modest contribution to the total width, from our theoretical estimates we would deduce $\boldsymbol{\Gamma_H < 38\ GeV}$.
- Finally, the CMS and TOTEM collaborations have been searching for high-mass photon pairs produced in **pp** diffractive scattering, i.e., when both final protons are tagged and have large $\mathbf{x_F}$. In the range of invariant masses $\mathbf{650\,(40)\ GeV}$ and for a statistics of $\mathbf{102.7\ fb^{-1}}$, the observed number of $\gamma\gamma$ events is $\mathbf{N_{obs} \sim 76\,(9)}$, to be compared with an estimated background $\mathbf{N_B \sim 40\,(9)}$, which is quoted as being the best estimate by CMS. In the most conservative case, viz. $\mathbf{N_B = 49}$, this is a local $\mathbf{3\sigma}$ effect and the only significant excess in the plot, shown in Fig. 11.

Figure 10

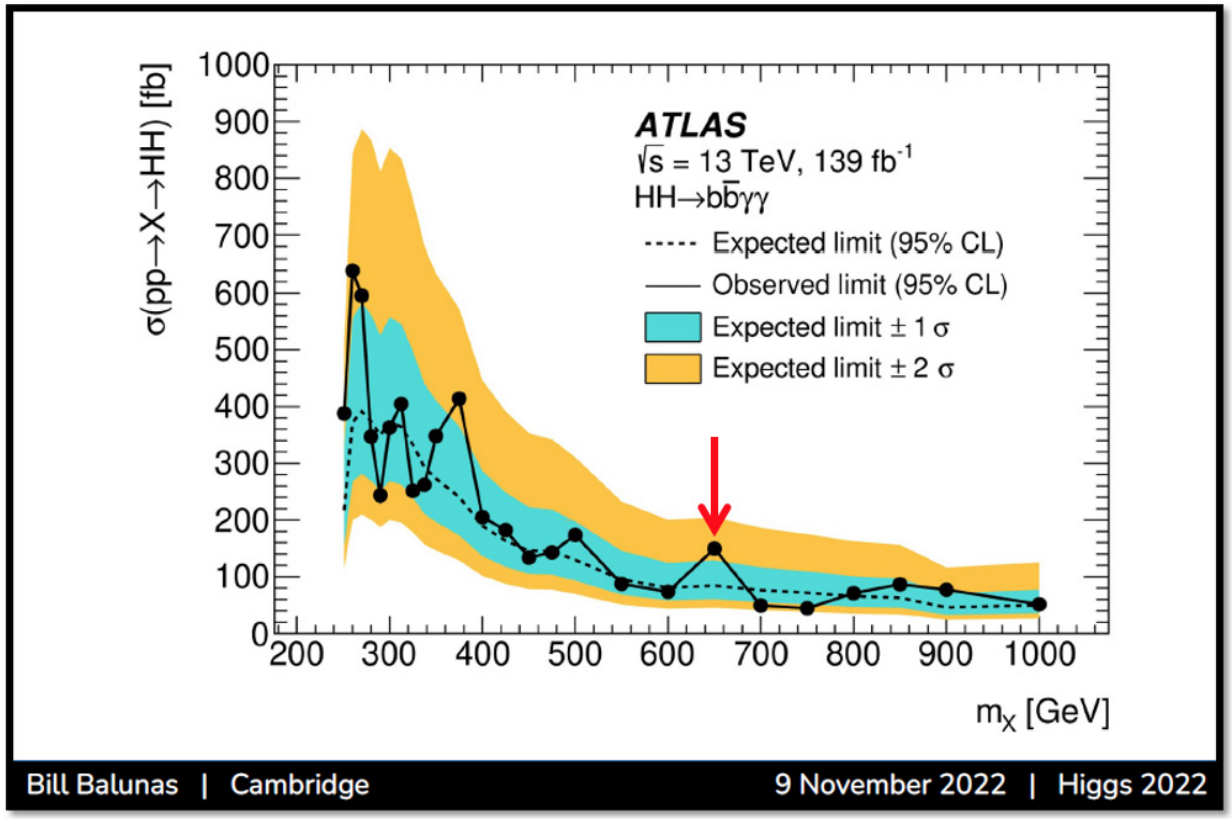

Expected and observed 95% upper limit for the cross section $\sigma(pp \to X \to h(125)h(125))$ extracted by ATLAS in Phys. Rev. D **106**, 052001 (2022) from the final state $(b\bar{b} + \gamma\gamma)$.
The figure is taken from the talk given by Bill Balunas at "Higgs 2022" and is the same as Fig. 15 in the PRD paper.

Figure 11

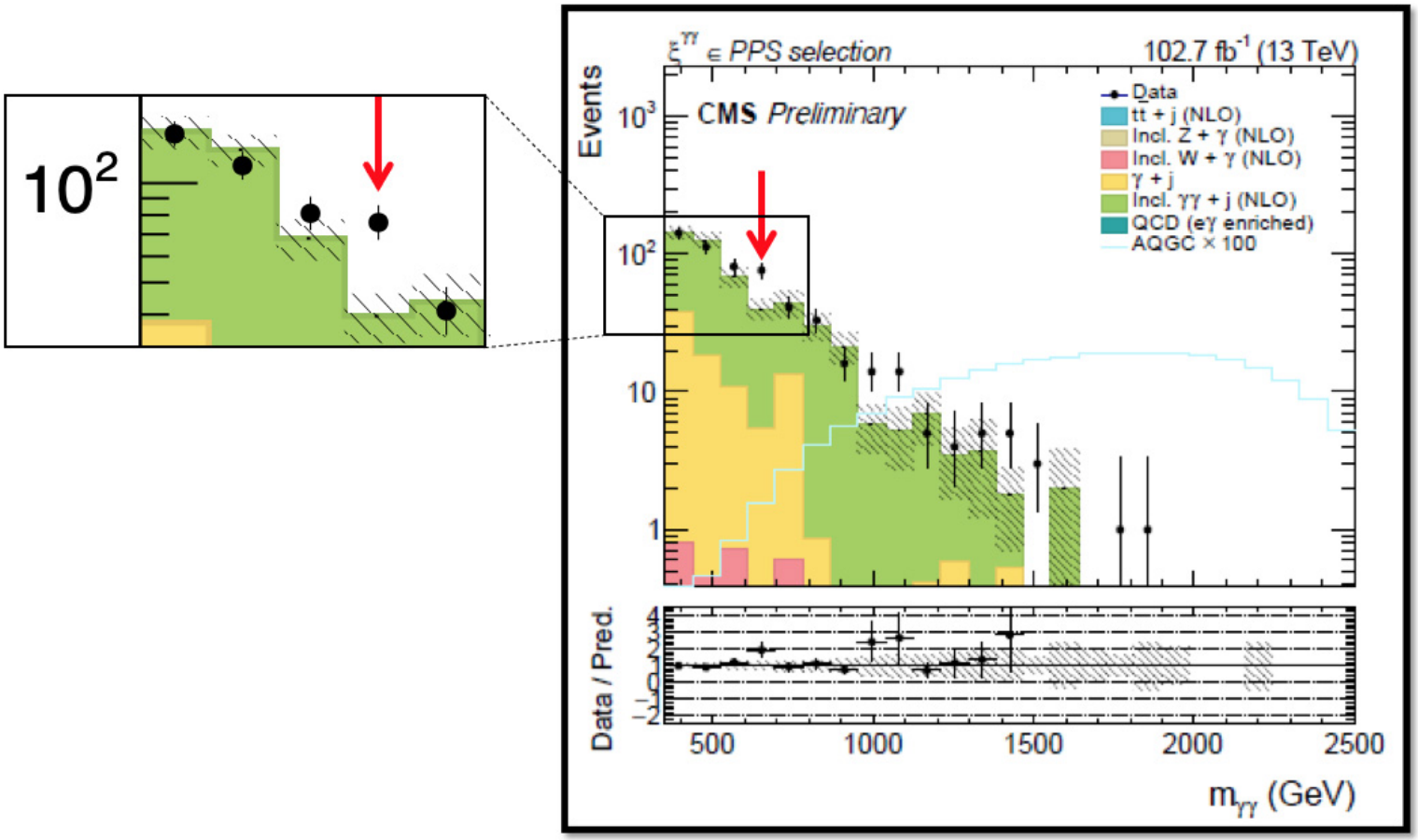

The number of $\gamma\gamma$ events produced in *pp* diffractive scattering, as reported by CMS in CERN Report nos. CMS-PAS-EXO-21-007, TOTEM-NOTE-2022-005. In the range 650 (40) GeV, the observed number was $N_{\rm obs} \sim 76\,(9)$, to be compared to an estimated background $N_{\rm B} \sim 40\,(9)$.

- **Summarising all the presented experimental indications:**

  $\Rightarrow$ The ATLAS 4-lepton data shown and analysed in Tables 2, 4, and 5 show deviations from the background with a definite excess-defect sequence, which could indicate the presence of a resonance. From the last column of these Tables, the combined statistical significance of the observed deviations can be estimated at the $\mathbf{3\sigma}$ level. A fit gives a good description of the data for a resonance mass $\mathbf{M_H = 677^{+30}_{-14}\ GeV}$.

  $\Rightarrow$ Observing the $\mathbf{+3\sigma}$ excess at **684 (16) GeV** in the inclusive ATLAS $\gamma\gamma$ events, a fit to these data was done in M. Consoli, L. Cosmai, F. Fabbri, 2208.00920; Universe **9** (2023) 99. The resulting mass was found to be $\mathbf{M_H = 696\ (13)\ GeV}$.

  $\Rightarrow$ An overall $\mathbf{+2\sigma}$ effect in the $\mathbf{(b\bar{b} + \gamma\gamma)}$ channel is obtained by combining the excess of ATLAS events at **650 (25) GeV** and the corresponding excess by CMS at **675 (25) GeV**.

  $\Rightarrow$ A $\mathbf{+3\sigma}$ excess at **650 (40) GeV** is found in the distribution of CMS-TOTEM $\gamma\gamma$ events from **pp** diffractive scattering.

IV. Unitary coupled-channel formalism for h(125)+H(700)

- In order to accurately study the resonance properties of a possible additional Higgs boson **H** with a mass of about 700 GeV and an estimated width of a few tens of GeV requires a unitary coupled-channel formalism.
- The main reason is the inevitable mixing of **H** with the observed light Higgs at 125 GeV (to be denoted by **h**) owing to their common decay channels, even if these are of a subthreshold nature in the latter case. Preliminary results indicate that this mixing may significantly reduce the **H** width.
- If we assume that the dominant decays are of the two-body type, most importantly $\mathbf{t\bar{t}}$ but also $\mathbf{W^{\pm}W^{\mp}}$, **ZZ**, and **hh**, then the Resonance-Spectrum Expansion (RSE) comes to mind.
- The RSE approach was developed as a solvable multichannel model for non-exotic meson spectroscopy, formulated in momentum space, which treats all mesons as bound-state or resonance poles in a coupled-channel **S-matrix** for meson-meson scattering. It is diagrammatically represented by the upper figure in Fig. 12.

Figure 12

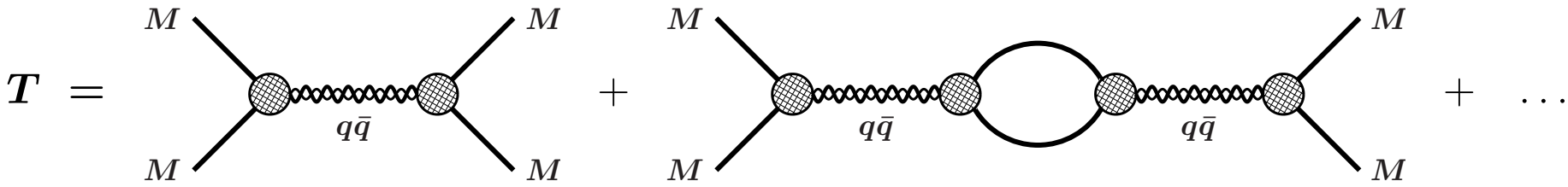

Graphical depiction of RSE T-matrix for non-exotic two-meson scattering. For references, see e.g.

E. van Beveren, G. Rupp, Annals Phys. **324** (2009) 1620

S. Coito, G. Rupp, E. van Beveren, Phys. Rev. D **80** (2009) 094011

Figure 13

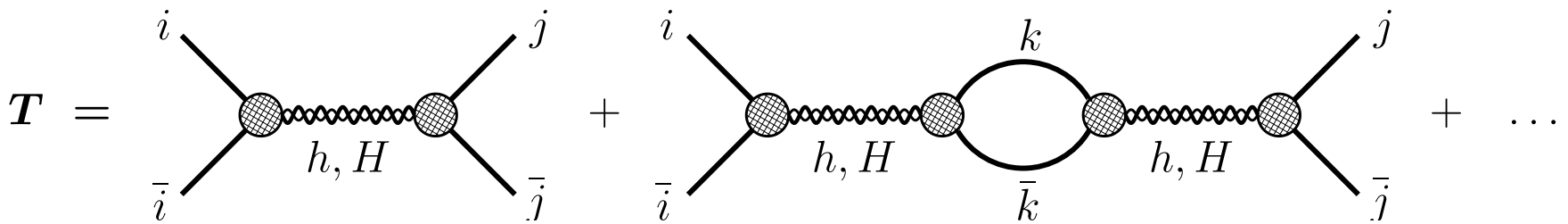

Graphical depiction of the RSE T-matrix for two Higgs-field mass states h and H. The labels i, j, k and $\bar{i}, \bar{j}, \bar{k}$ at the external legs and the loop stand for $(t/\bar{t}, W^{\pm}, Z, h)$ and $(\bar{t}/t, W^{\mp}, Z, h)$, respectively.

- The bubble sums in Figs. 12 and 13 allows to solve algebraically the fully off-shell multichannel **T-matrix** in the framework of a relativistic Lippmann–Schwinger-type equation, due to the separability of the effective interaction.
- In Fig. 12, the intermediate-state propagator stands for a tower of bare $\mathbf{q\bar{q}}$ states with the same quantum numbers. This propagator couples to the incoming and outgoing two-meson states via a vertex representing $\mathbf{q\bar{q}}$ creation or annihilation. With a choice for the vertex function based on the $^3\mathbf{P_0}$ model, the **T-matrix** can be solved analytically as well and so also the **S-matrix** defined as $\mathbf{S} \equiv \mathbb{1} + 2\,\mathbf{i}\,\hat{\mathbf{T}}$, where the hat stands for "fully on-shell".
- Figure 13 depicts a similar situation, but now for bare **h** and **H** coupling to $\mathbf{t\bar{t}}$, $\mathbf{W^{\pm}W^{\mp}}$, **ZZ**, and **hh** in the initial/final state.
- Contrary to the meson case, we do not know of any substructure of **h** and **H**, so the loops in the bubble sum are in principal logarithmically divergent. So we regularise the loops, in an effective sense, by taking a convenient form factor for the vertex functions. This will introduce a yet to-be-studied parameter dependence.

V. Summary and Conclusions

- In the foregoing, theoretical, lattice, and experimental indications have been presented that all point to the existence of second resonance of the Higgs field, with a mass close to **700 GeV.**
- The non-perturbative approach to ϕ^4 theory, based on different yet equivalent forms of the effective potential, allows to avoid the inconvenient occurrence of a second minimum of the effective potential far beyond the Planck scale and much deeper than the EW vacuum. It also provides for a more consistent reconciliation with the assumed triviality of the continuum theory.
- Lattice simulations of ϕ^4 theory in the Ising limit support our interpretation of SSB as a weak first-order phase transition, while also providing for an upper mass bound in the case of a single Higgs boson that is compatible with our range of **H** masses.
- The combined local $+\mathbf{3}\sigma$ and $+\mathbf{2}\sigma$ signals in various ATLAS and CMS data, indicating a resonance in the range **650–700 GeV**, have a significance of at least $+\mathbf{5}\sigma$. This cannot be downgraded by the *"look elsewhere"* effect, in view of our definite prediction.

شكرًا لكم على اهتمامكم